Jet tomography in heavy ion collisions with deep learning

Yi-Lun Du,[1,*] Daniel Pablos,[2,†] and Konrad Tywoniuk[1,‡]

[1] *Department of Physics and Technology, University of Bergen, Postboks 7803, 5020 Bergen, Norway*
[2] *INFN, Sezione di Torino, via Pietro Giuria 1, I-10125 Torino, Italy*

Deep learning techniques have the power to identify the degree of modification of high energy jets traversing deconfined QCD matter on a jet-by-jet basis. Such knowledge allows us to study jets based on their initial, rather than final energy. We show how this new technique provides unique access to the genuine configuration profile of jets over the transverse plane of the nuclear collision, both with respect to their production point and their orientation. Effectively removing the selection biases induced by final-state interactions, one can in this way analyse the potential azimuthal anisotropies of jet production associated to initial-state effects. Additionally, we demonstrate the capability of our new method to locate with remarkable precision the production point of a dijet pair in the nuclear overlap region, in what constitutes an important step forward towards the long term quest of using jets as tomographic probes of the quark-gluon plasma.

Introduction. Jets are collimated sprays of hadrons that are produced in hard QCD processes in high-energy particle collisions. Within the context of heavy-ion collisions, they are witnesses to the creation of deconfined QCD matter, known as the quark-gluon plasma (QGP). This new state of matter, which is believed to have filled the Universe during the first microseconds after the Big Bang, behaves as the most perfect liquid ever measured in Nature [1–3]. During their passage through this medium, partonic jet modes are subject to momentum diffusion and energy loss by the radiation of soft quanta towards large angles, a phenomenon known as jet quenching [4–7]. Key information about the medium is contained in the detailed modification of these hard probes, turning them into essential tools on which tremendous theoretical and experimental effort is being devoted [8–13].

In practice, a jet is defined through a reconstruction algorithm with an associated parameter R that can be interpreted as an angular size. The momenta of the collection of particles that belong to the jet are recombined, usually using sequential addition of four-momenta, to determine the kinematics of the jet itself. They possess an internal structure, a recognizable organization pattern of the particles within, which is well understood in vacuum [14–16]. For instance, the individual splittings that make up the tree-structure of a jet can also be associated with a timescale [17], given by the quantum-mechanical formation time [18]. Finally, in infrared and collinear safe substructure observables, non-perturbative effects are strongly mitigated allowing for a direct access to the perturbative structure of jets. For these reasons, jets offer a special advantage with respect to individual hadrons.

Using jets as differential probes of the spatio-temporal structure of the QGP created in heavy-ion collisions, aka *jet tomography*, is a long-standing goal. On a jet-by-jet basis it is evident that the modifications induced by the medium follow from the local properties sampled along the jet trajectory from the hard production point out to the detector. The ability to unambiguously gauge the effect from the QGP on this level would lead to unprecedented precision in determining local properties of the fluid, including flow [19, 20], path-length dependence of modifications [21] and the possibility of observing deconfined quasi-particle degrees of freedom in the QGP [22–24]. Nonetheless, tomographic analyses on the level of inclusive jet populations have been hindered by intrinsic biases that accentuate samples experiencing small modifications over samples that are strongly affected [25]. Such biases arise due to the steeply falling spectrum of jet initiator transverse momenta and strongly distort the magnitude of medium effects, e.g. the in-medium path-length distribution of surviving jets.

In this Letter, we propose a technique based on deep learning that mitigates these bias effects and results in a better control of the path-length traversed by individual jets based on their level of modification. Given a measured jet at p_T and cone size R, the procedure allows us to estimate with reasonable accuracy the transverse momentum $p_T^{\rm initial}$ the jet would have had, had it not interacted with a medium, see [26] for further details on how to establish such a correspondence. The technique uses only the information of the hadrons that are contained in the reconstructed jet and is easily adaptable to other model studies.

Having at hand an estimate of how much energy an individual jet has lost is a powerful tool that allows for many interesting applications. It was previously used to reveal more pronounced substructure modifications of jets [26] by constructing ratio observables for specific jet samples where one compares jets in proton-proton and heavy-ion collisions with the same *initial* p_T instead of comparing them at a fixed *final* p_T, as conventionally done. We refer to these two jet selections as *initial energy selection* (IES) and *final energy selection* (FES), respectively. Here, we demonstrate the usefulness of our approach to tomographic applications in two concrete examples. The first deals with reconstructing the true distribution of path-lengths that jets experience, eliminating the effects of "surface bias" [27–29]. The genuine

nuclear density distributions that influence the hard process production point are in this way revealed. Moreover, possible initial-state effects that lead to anisotropy in the jet azimuthal orientation distribution could thereby be exposed. The second application combines the extraction of the lost energy with accessible knowledge about the orientation of the jet with respect to the event plane of the collision, as determined by the dominant azimuthal harmonic v_2 of the particle distribution. We can, in this manner, constrain the path length dependence separately for jets traveling in and transverse to the event plane of the collisions, refining the path to experimentally pinning down the original production point of a dijet pair. We expect this new development to importantly contribute to the set of tools aimed at the exploitation of energetic jets as tomographic probes of the QGP.

Quantifying energy loss jet-by-jet. In vacuum, high energy partons produced in a hard QCD collision relax their typically large virtuality down to the hadronization scale via successive splittings. The description of these processes are well controlled both from theory [30–32] and within Monte Carlo parton shower generators [33] through the appropriate implementation of the DGLAP evolution equations. It has been shown that there is a phase space region of an in-medium parton shower that occurs as in vacuum, as it takes place before any medium induced modifications have had the time to develop [34–36]. In terms of the relative transverse momentum of a splitting, it corresponds to the regime $\langle k_\perp^2\rangle_{\rm med} \ll k_\perp^2 \ll (p_T R)^2$, where $\langle k_\perp^2\rangle_{\rm med}$ is the typical momentum broadening induced by medium interactions and $\sim p_T R$ is the scale of the jet. This allows one to ask the question of which would have been the energy of a jet in the absence of final-state effects. Within an angular ordered picture for the vacuum parton shower, the first emission off the primary parton to be within the cone angle R sets the fraction of energy contained in the jet with respect to the energy of the parton shower initiator. In the leading-logarithmic approximation, it is legitimate to assume that the in-cone emissions that belong to the vacuum-like dominated region, given by the condition above, already define the energy of the jet before medium modifications become relevant. The presence of the medium alters this fairly developed structure, typically leading to energy loss due to transport of particles out of the jet cone.

Within this factorised picture, we can define what we call the energy loss ratio $\chi \equiv p_T/p_T^{\rm initial}$ as the ratio between the jet transverse momentum in the medium, or simply p_T, and the one it would have had in the absence of the medium, which we call $p_T^{\rm initial}$. In Ref. [26] we describe the matching procedure carried out at hadron level necessary to establish this connection between a quenched jet and its vacuum-like counterpart. In our previous and current work, we use the hybrid strong/weak coupling model [37, 38] for the generation of the quenched jets, which combines perturbative physics for high virtuality parton evolution [39] and non-perturbative insights from holography for the jet-medium interaction [40, 41]. At strong coupling, the deposition of energy and momentum in the QGP generates a wake [42] that decays into hadrons at the freeze-out hypersurface, effectively transporting the jet energy towards large angles in the form of soft particles [43]. We extract χ on a jet-by-jet basis by using jet images as inputs to a convolutional neural network (CNN), achieving a good degree of accuracy across a wide range in χ. We refer the interested readers to our previous paper [26] for further details on data preprocessing and software architecture (see also [44] for a complementary approach). In this work we focus instead on some of the novel applications that are now available to us.

Factoring out final-state effects. In nucleus-nucleus collisions, the production of hard processes can be described by the Glauber model [45, 46], where the rate of collisions is governed by the inelastic cross section of nucleon-nucleon scatterings and the density of nucleons are described by the Woods-Saxon distribution. The distribution of production points is naturally strongly correlated with the distribution of path-lengths experienced by the entire jet population. However, jets that experience final-state interactions will tend to be more modified, and experience, on average, more energy loss, if they originate from production points deep within the nuclear overlap region rather than from the surface. Therefore, selecting a jet population based on their *final*, measured transverse momenta will bias the jet selection toward short path-lengths, and small energy losses, leading to a "surface bias" [27–29]. In contrast, focusing on the original jet population, or selecting jets according to their *initial* transverse momentum, accessed with $p_T^{\rm initial} = p_T/\chi$, should recover the true path-length distribution associated to the underlying nuclear overlap density.

In order to visualize these aspects, we generate dijet events at $\sqrt{s_{NN}} = 5.02$ TeV for PbPb collisions in the 0-5% centrality bin corresponding to around 700,000 samples of inclusive jets reconstructed with anti-k_t [47] and radius parameter $R = 0.4$ using FastJet [48]. In the left column of Fig. 1 we show the production point density of the hard QCD processes in the transverse plane using three different jet selections. In the top left panel, we select jets with a measured momentum $p_T > 200$ GeV and plot the location where they were produced (taken directly from the model). This selection, referred to as FES, is the only possible setup in experiments without the knowledge of χ. Taking the difference with respect to the actual production point density using the Glauber model in the top right plot of Fig. 1 we observe that, compared to the true geometrical distribution according to which the jets were produced, there is a relative absence of jets produced at the centre of the overlap region. This clearly shows how, due to the presence of a steeply falling

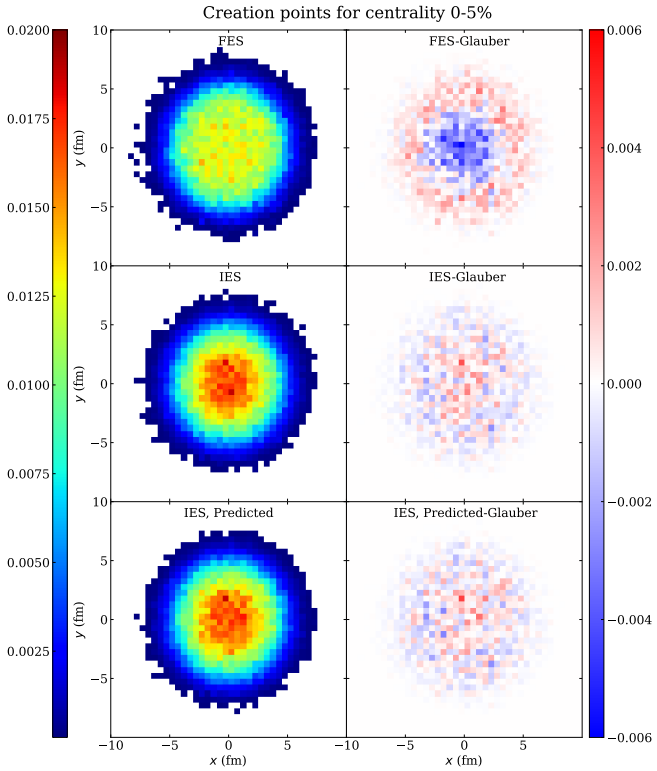

FIG. 1. Left: Probability distribution of the production point in the transverse plane of a hard QCD process when using the FES setup, in the top, versus when IES setup is used, with true χ in the middle and with predicted χ^p in the bottom. Right: Difference of the results of the left column with respect to the distribution obtained by directly using the Glauber procedure.

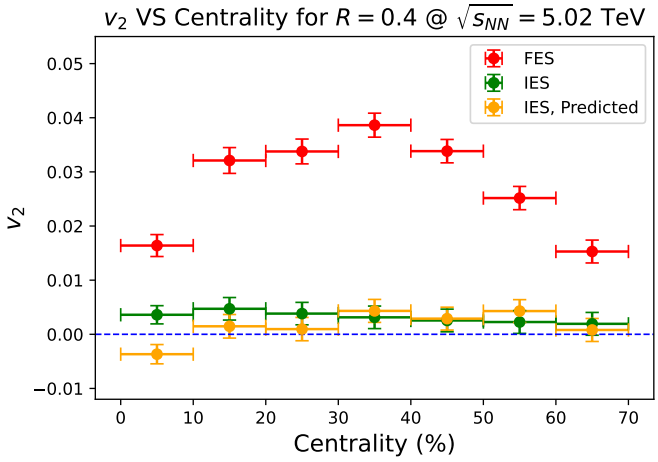

FIG. 2. Centrality dependence of v_2 for FES setup (red) and IES setup with true χ (green) and predicted χ^p (orange).

spectrum, imposing a p_T cut on the measured jet energy naturally selects jets that have lost the least energy.

With a good estimate of the energy loss ratio χ we can, however, perform a different jet selection. In the middle and bottom left plots of Fig. 1 we show the jet production points (again, supplied by the model) for the so-called initial energy selection (IES) with true χ, i.e. extracted directly from model data, and predicted χ^p, i.e. extracted by the trained CNN, respectively, where we only include those jets with $p_T^{\text{initial}} > 200$ GeV (additionally, we demand that $p_T > 100$ GeV because this corresponds to the kinematical range where we have trained our neural network). In other words, we explicitly count jets that initially have a sufficiently large p_T^{initial} to enter the selection but, due to energy loss, eventually are not counted. Remarkably, the differences with respect to the Glauber distribution, shown in the middle and bottom right panels, both display no sizeable deviation beyond random noise. We have also checked that this agreement does not depend on the precise cut on p_T as long as it is sufficiently below the cut of p_T^{initial}. This demonstrates that, by employing IES, we are able to mitigate all final-state effects, such as medium-induced energy loss, and we obtain a jet population that reflects the true path-length distribution experienced in a heavy-ion collision.

Selection bias effects, that we discussed in detail above, affect not only the creation point distribution in the transverse plane but also the jet orientation with respect to the event plane of the collision [49]. In contrast to the production points shown in Fig. 1, the azimuthal distribution of particle production can be measured in experiments and quantified by the harmonic coefficients $v_n = \langle \exp[i\, n\phi] \rangle$, where ϕ is the azimuthal angle with respect to the event plane and the average is taken over all measured events. In particular, for high-p_T probes, the second harmonic coefficient v_2 is given directly by

$$v_2 = \left\langle \frac{p_{T,x}^2 - p_{T,y}^2}{p_{T,x}^2 + p_{T,y}^2} \right\rangle \tag{1}$$

where $p_{T,x} = p_T \cos\phi$ and $p_{T,y} = p_T \sin\phi$ are the jet momenta in the x and y directions with respect to the event plane. These momentum anisotropies can emerge both due to initial-state correlations and final-state interactions [50, 51]. The former arise from quantum interference in the incoming nuclear wave-functions and dominate the observable signal of v_2 only at small multiplicities [52]. The latter are generally driven by the geometry of the collisions (the nuclear positions within the nuclei at a given impact parameter). The p_T and centrality dependence of the v_n coefficients have been instrumental in providing detailed information about the properties of the QGP from bulk particle production [53–55]. For high-p_T hadrons and jet production, azimuthal anisotropies are again mainly driven by the path-dependence of energy loss.

We show results for jet v_2 from the hybrid strong/weak coupling model in Fig. 2 in PbPb collisions at $\sqrt{s_{NN}} = 5.02$ TeV, using anti-k_t and $R = 0.4$, as a function of

centrality. The red dots correspond to the obtained v_2 using FES (we have checked that the results from the hybrid model reproduce experimental data on high-p_T v_2 at $\sqrt{s_{NN}} = 2.76$ TeV [56] very well, see the supplemental material for more details). As the nuclear overlap region becomes more and more anisotropic with increasing impact parameter (increasing the centrality class), final-state energy loss effects increasingly enhance the relative contribution of the less quenched jets that propagate along the short axis of the collision. Thus, $v_2^{\rm FES}$ is positive and grows with centrality. However, as the medium becomes smaller and colder at the most peripheral collisions, energy loss is reduced and v_2 consistently decreases.

On the other hand, the green and orange points in Fig. 2 correspond to the results for the IES procedure using the true and predicted values of χ, respectively, with selection criteria as chosen in Fig. 1. By removing the selection bias effect we reveal the initial-state orientation of hard jets in our model which, by construction, is random and therefore $v_2^{\rm IES}$ is consistent with zero. Remarkably, the agreement between the green and orange dots demonstrates that our algorithm, having been trained on jets in the 0-5% centrality class, is generalizable across centrality classes. We also note that our method would have yielded $v_2^{\rm IES} \neq 0$ and revealed any remaining anisotropy associated to other hypothesized mechanisms, such as quantum correlations in the initial wave functions [57–61] or other quantum interference effects [62, 63][64]. While such effects at high-p_T are expected to be small within current models, finding evidence of such *additional* anisotropies in nucleus-nucleus collisions would support the idea of a common, underlying contribution to collective behavior across different system sizes.

Jet tomography of the QGP. Jets in heavy-ion collisions have been proposed as tomographic probes of the QGP since the beginning of the field [28, 29, 65, 66]. One of the main ideas has consisted in contrasting the distribution of production points, and related distribution of in-medium path-lengths, of different hard probe samples, for instance inclusive jets (or hadrons) in dijet events versus semi-inclusive boson-jet (or boson-hadron) samples, on which the selection bias has a different effect due to the different associated jet production spectrum. More recently, a new technique called gradient jet tomography has been developed, which exploits the correlation between the original production point and the asymmetry in the transverse momentum distribution, with respect to the jet direction, of partons in the cone caused by the spatial gradient of the jet quenching parameter $\widehat{q}$ [67]. Getting access to this information is a key step towards future, more focused studies in which the modifications of quenched jets can provide detailed aspects of the properties of the QGP along its propagation path.

We now turn to the final application of our tomographic studies using deep learning. Having established that we can restore the true path-length distribution of jets above, we can further narrow down the path-length selection by choosing jets within a class of energy loss ratios, i.e. by choosing jets in a specific range of χ. However, due to the many sources of fluctuations (from jet substructure fluctuations to fluctuations residing in the medium interactions), the correlation between χ and the path length is not as strong as one could have expected [26, 68]. Here we propose that the path-length distribution, and consequently the possible production points in the nuclear overlap area, can be constricted further by additionally constricting the direction of the jet propagation with respect to the event plane of the collisions. Concretely, we will consider jets propagating in-plane, i.e. parallel to the event plane, and out-of-plane, i.e. transverse to the event plane.

By combining our knowledge of the orientation of a jet with respect to the event plane with the degree of energy loss χ, we present the localization of the production point of a given jet with a new level of precision. In Fig. 3 we show results for around 900,000 jets, generated at $\sqrt{s_{NN}} = 5.02$ TeV for PbPb collisions at 30-40% centrality and reconstructed using anti-k_t and $R = 0.4$. In the upper (lower) row we have selected jets that are propagating in-plane (out-of-plane), which means they are approximately oriented along the short (long) axis of the nuclear overlap region. This corresponds to jets with distinctly positive (negative) v_2. In the bottom of each sub-figure in the upper (lower) row we also plot the average nuclear overlap density, represented by the in-plane (out-of-plane) jet production point distribution for FES inclusive in χ, which has been rotated so that the event plane, and impact parameter vector, points along the x-direction.

We can further slice the selection depending on which sense the jet is propagating: either left (in blue) or right (in red) for the in-plane jets, and either up (in orange) or down (in green) for the out-of-plane jets. The histograms in each of the first three columns display the creation point density for jets belonging to a given range of the predicted energy loss ratio χ^p. Finally, the fourth column shows the results inclusive in predicted χ^p and corresponds to the production point distributions if we had no knowledge of the degree of in-medium modification. Even though there is some degree of separation of the production point distributions for the χ-inclusive jet selection, a large degree of overlap can be noticed. This situation changes radically by using our knowledge of predicted χ^p on a jet-by-jet basis [69]. The third column in Fig. 3 shows results for fairly unquenched jets, with $0.95 < \chi^p < 1$. In order to belong to this class, a jet propagating upwards (focusing first on the out-of-plane jets in the lower row) has to have traversed merely a short distance through the QGP and therefore its production point is predominantly localized in the *upper* part

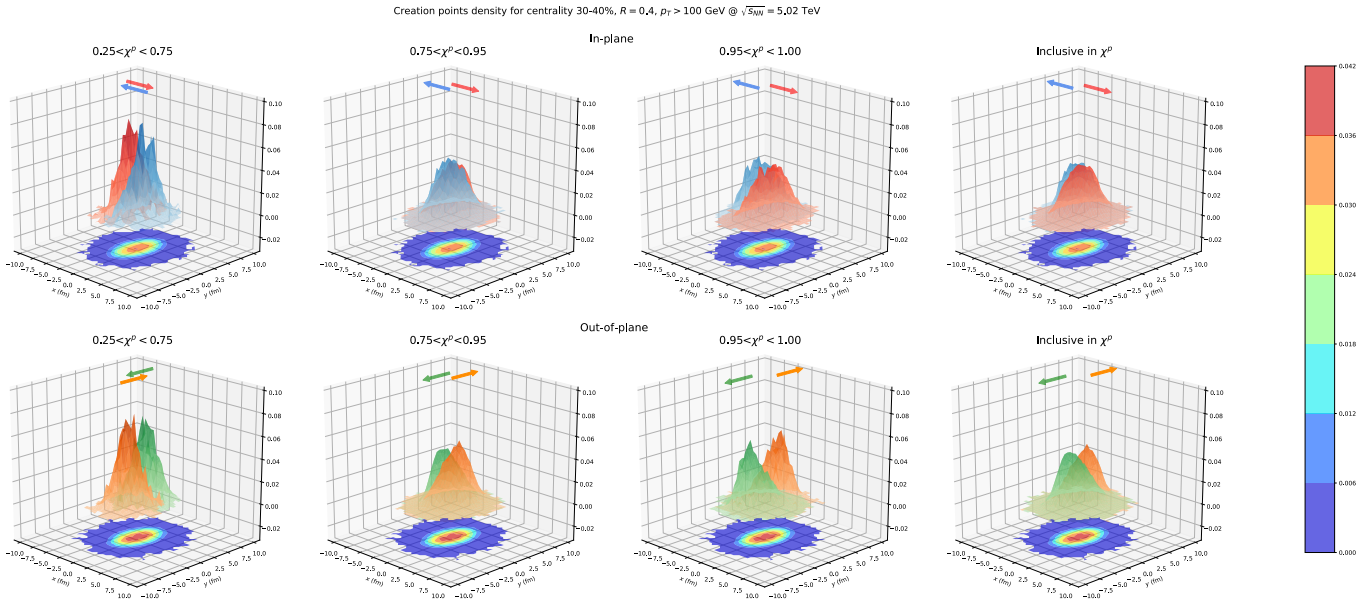

FIG. 3. Creation point distributions in the transverse plane for the jets in 30-40% centrality and inclusive and sliced in different ranges of the predicted χ^p in four columns, respectively. The in-plane jets going left (blue) and right (red) are shown in the upper row and the out-of-plane jets going up (orange) and down (green) are shown in the lower row. The 2-D histogram in the bottom of each plot is the distribution of the inclusive in-plane (upper row) and out-of-plane (lower row) jets in this centrality.

of the overlap region (and vice versa for a jet propagating downwards). This reasoning also applies, in reverse, for jets belonging to the very quenched class, with $0.25 < \chi^p < 0.75$, displayed in the leftmost column. In this case, a very quenched jet propagating upwards will have needed to traverse a long distance in the QGP, or analogously through a hot region, and consequently its production point will instead be predominantly localized in the *lower* hemisphere (and vice versa for the downward propagating case). Obviously, analogous arguments also apply for the in-plane cases plotted in the upper row of Fig. 3. The second column shows the notably overlapping transition region that bridges the gap between the fairly unquenched and very quenched classes of columns one and three, respectively.

Conclusions. In this Letter, we demonstrate the power of deep learning techniques to pin down the genuine nuclear density distributions that affect high-p_T jet production in the transverse plane and the initial-state jet azimuthal anisotropies, quantifiable through the elliptic flow coefficient v_2, by learning the amount of energy loss χ on a jet-by-jet basis. In both cases, the final-state effects induced by the selection bias can be removed to a large extent by selecting jets according to their initial transverse momenta. We have argued that extracting the possible initial-state anisotropies in nucleus-nucleus collisions can serve to clarify the origin of the high-p_T v_2 measured in small systems, which currently seems in strong conflict with an explanation based solely on energy loss physics.

Furthermore, by selecting jets according to the sign of v_2, we have shown the capability of our method to locate the jet creation point in the transverse plane with remarkable precision, representing a significant development towards using jets as tomographic probes of the QGP. To move forward, it will be necessary to study the generalizability of our novel framework by testing the prediction performance of χ when applied to different energy loss models. The interplay between the jet and the local properties of the medium, such as the local hydrodynamic flow [19, 20, 70–72] or temperature and density gradients [20, 67], which determine preferred directions and deformed radiation spectra for the soft quanta emitted from the jet, are ingredients that are still missing from the current version of the model used in this work. This extra layer of information, which improves per se the tomographic power of quenched jets, could also be used to greatly improve the prediction performance of χ and even allow for a direct extraction of the traversed length in the QGP, a challenging task that will be tackled in future work.

Acknowledgements. This work is supported by the Trond Mohn Foundation under Grant No. BFS2018REK01 and the University of Bergen. Y. D. thanks the support from the Norwegian e-infrastructure UNINETT Sigma2 for the data storage and HPC resources with Project Nos. NS9753K and NN9753K. D.P. has received funding from the European Union's Horizon 2020 research and innovation program under the Marie Skłodowska-Curie grant agreement No. 754496.

* yilun.du@uib.no
† daniel.pablos.alfonso@to.infn.it
‡ konrad.tywoniuk@uib.no

[1] K. Ackermann, N. Adams, C. Adler, Z. Ahammed, S. Ahmad, C. Allgower, J. Amsbaugh, M. Anderson, E. Anderssen, H. Arnesen, *et al.*, Phys. Rev. Lett **86**, 402 (2001).
[2] K. Aamodt, B. Abelev, A. A. Quintana, D. Adamova, A. Adare, M. Aggarwal, G. A. Rinella, A. Agocs, S. A. Salazar, Z. Ahammed, *et al.*, Phys. Rev. Lett **105**, 252302 (2010).
[3] K. Aamodt, B. Abelev, A. A. Quintana, D. Adamova, A. Adare, M. Aggarwal, G. A. Rinella, A. Agocs, A. Agostinelli, S. A. Salazar, *et al.*, Phys. Rev. Lett **107**, 032301 (2011).
[4] D. d'Enterria, Landolt-Bornstein **23**, 471 (2010), arXiv:0902.2011 [nucl-ex].
[5] A. Majumder and M. Van Leeuwen, Prog. Part. Nucl. Phys. **66**, 41 (2011), arXiv:1002.2206 [hep-ph].
[6] Y. Mehtar-Tani, J. G. Milhano, and K. Tywoniuk, Int. J. Mod. Phys. A **28**, 1340013 (2013), arXiv:1302.2579 [hep-ph].
[7] J.-P. Blaizot and Y. Mehtar-Tani, Int. J. Mod. Phys. E **24**, 1530012 (2015), arXiv:1503.05958 [hep-ph].
[8] B. Abelev *et al.* (ALICE), JHEP **03**, 013 (2014), arXiv:1311.0633 [nucl-ex].
[9] J. Adam *et al.* (ALICE), Phys. Lett. B **746**, 1 (2015), arXiv:1502.01689 [nucl-ex].
[10] G. Aad, B. Abbott, J. Abdallah, S. A. Khalek, O. Abdinov, R. Aben, B. Abi, M. Abolins, O. AbouZeid, H. Abramowicz, *et al.*, Phys. Rev. Lett. **114**, 072302 (2015).
[11] M. Aaboud *et al.* (ATLAS), Phys. Lett. B **774**, 379 (2017), arXiv:1706.09363 [hep-ex].
[12] M. Aaboud, G. Aad, B. Abbott, O. Abdinov, B. Abeloos, D. K. Abhayasinghe, S. H. Abidi, O. AbouZeid, N. Abraham, H. Abramowicz, *et al.*, Phys. Lett. B **790**, 108 (2019).
[13] S. Acharya *et al.* (ALICE), Phys. Rev. C **101**, 034911 (2020), arXiv:1909.09718 [nucl-ex].
[14] G. P. Salam, Eur. Phys. J. C **67**, 637 (2010), arXiv:0906.1833 [hep-ph].
[15] A. J. Larkoski, I. Moult, and B. Nachman, Phys. Rept. **841**, 1 (2020), arXiv:1709.04464 [hep-ph].
[16] S. Marzani, G. Soyez, and M. Spannowsky, *Looking inside jets: an introduction to jet substructure and boosted-object phenomenology*, Vol. 958 (Springer, 2019) arXiv:1901.10342 [hep-ph].
[17] H. A. Andrews *et al.*, J. Phys. G **47**, 065102 (2020), arXiv:1808.03689 [hep-ph].
[18] Y. L. Dokshitzer, V. A. Khoze, A. H. Mueller, and S. I. Troian, *Basics of perturbative QCD* (1991).
[19] N. Armesto, C. A. Salgado, and U. A. Wiedemann, Phys. Rev. C **72**, 064910 (2005), arXiv:hep-ph/0411341.
[20] A. V. Sadofyev, M. D. Sievert, and I. Vitev, (2021), arXiv:2104.09513 [hep-ph].
[21] B. Betz and M. Gyulassy, JHEP **08**, 090 (2014), [Erratum: JHEP 10, 043 (2014)], arXiv:1404.6378 [hep-ph].
[22] F. D'Eramo, K. Rajagopal, and Y. Yin, JHEP **01**, 172 (2019), arXiv:1808.03250 [hep-ph].
[23] J. a. Barata, Y. Mehtar-Tani, A. Soto-Ontoso, and K. Tywoniuk, (2020), arXiv:2009.13667 [hep-ph].
[24] M. Cè, T. Harris, H. B. Meyer, and A. Toniato, JHEP **03**, 035 (2021), arXiv:2012.07522 [hep-ph].
[25] R. Baier, Y. L. Dokshitzer, A. H. Mueller, and D. Schiff, JHEP **09**, 033 (2001), arXiv:hep-ph/0106347.
[26] Y.-L. Du, D. Pablos, and K. Tywoniuk, JHEP **21**, 206 (2020), arXiv:2012.07797 [hep-ph].
[27] A. Dainese, C. Loizides, and G. Paic, Eur. Phys. J. C **38**, 461 (2005), arXiv:hep-ph/0406201.
[28] H. Zhang, J. F. Owens, E. Wang, and X.-N. Wang, Phys. Rev. Lett. **98**, 212301 (2007), arXiv:nucl-th/0701045.
[29] H. Zhang, J. F. Owens, E. Wang, and X.-N. Wang, Phys. Rev. Lett. **103**, 032302 (2009), arXiv:0902.4000 [nucl-th].
[30] M. Dasgupta, F. Dreyer, G. P. Salam, and G. Soyez, JHEP **04**, 039 (2015), arXiv:1411.5182 [hep-ph].
[31] M. Dasgupta, F. A. Dreyer, G. P. Salam, and G. Soyez, JHEP **06**, 057 (2016), arXiv:1602.01110 [hep-ph].
[32] Z.-B. Kang, F. Ringer, and I. Vitev, JHEP **10**, 125 (2016), arXiv:1606.06732 [hep-ph].
[33] S. Alioli *et al.*, (2019), arXiv:1902.01674 [hep-ph].
[34] Y. Mehtar-Tani and K. Tywoniuk, Phys. Rev. D **98**, 051501 (2018), arXiv:1707.07361 [hep-ph].
[35] P. Caucal, E. Iancu, A. H. Mueller, and G. Soyez, Phys. Rev. Lett. **120**, 232001 (2018), arXiv:1801.09703 [hep-ph].
[36] F. Domínguez, J. G. Milhano, C. A. Salgado, K. Tywoniuk, and V. Vila, Eur. Phys. J. C **80**, 11 (2020), arXiv:1907.03653 [hep-ph].
[37] J. Casalderrey-Solana, D. C. Gulhan, J. G. Milhano, D. Pablos, and K. Rajagopal, JHEP **2015**, 175 (2015).
[38] J. Casalderrey-Solana, D. C. Gulhan, J. G. Milhano, D. Pablos, and K. Rajagopal, JHEP **03**, 053 (2016), arXiv:1508.00815 [hep-ph].
[39] T. Sjostrand, S. Mrenna, and P. Z. Skands, Comput. Phys. Commun. **178**, 852 (2008), arXiv:0710.3820 [hep-ph].
[40] P. M. Chesler and K. Rajagopal, Phys. Rev. D **90**, 025033 (2014), arXiv:1402.6756 [hep-th].
[41] P. M. Chesler and K. Rajagopal, JHEP **05**, 098 (2016), arXiv:1511.07567 [hep-th].
[42] P. M. Chesler and L. G. Yaffe, Phys. Rev. Lett. **99**, 152001 (2007), arXiv:0706.0368 [hep-th].
[43] J. Casalderrey-Solana, D. Gulhan, G. Milhano, D. Pablos, and K. Rajagopal, JHEP **03**, 135 (2017), arXiv:1609.05842 [hep-ph].
[44] L. Apolinário, N. F. Castro, M. Crispim Romão, J. G. Milhano, R. Pedro, and F. C. R. Peres, (2021), arXiv:2106.08869 [hep-ph].
[45] A. Białas, M. Bleszyński, and W. Czyż, Nucl. Phys. B **111**, 461 (1976).
[46] M. L. Miller, K. Reygers, S. J. Sanders, and P. Steinberg, Annu. Rev. Nucl. Part. Sci. **57**, 205 (2007).
[47] M. Cacciari, G. P. Salam, and G. Soyez, JHEP **04**, 063 (2008), arXiv:0802.1189 [hep-ph].
[48] M. Cacciari, G. P. Salam, and G. Soyez, Eur. Phys. J. C **72**, 1896 (2012), arXiv:1111.6097 [hep-ph].
[49] U. A. Wiedemann, in *2007 European School of High-Energy Physics* (2008).
[50] H. Petersen, R. La Placa, and S. A. Bass, J. Phys. G **39**, 055102 (2012), arXiv:1201.1881 [nucl-th].
[51] M. Greif, C. Greiner, B. Schenke, S. Schlichting, and Z. Xu, Phys. Rev. D **96**, 091504 (2017), arXiv:1708.02076 [hep-ph].
[52] G. Giacalone, B. Schenke, and C. Shen, Phys. Rev. Lett. **125**, 192301 (2020), arXiv:2006.15721 [nucl-th].

[53] H. Niemi, G. S. Denicol, P. Huovinen, E. Molnar, and D. H. Rischke, Phys. Rev. Lett. **106**, 212302 (2011), arXiv:1101.2442 [nucl-th].

[54] J. Adam *et al.* (ALICE), Phys. Rev. Lett. **116**, 132302 (2016), arXiv:1602.01119 [nucl-ex].

[55] S. Ryu, J. F. Paquet, C. Shen, G. S. Denicol, B. Schenke, S. Jeon, and C. Gale, Phys. Rev. Lett. **115**, 132301 (2015), arXiv:1502.01675 [nucl-th].

[56] G. Aad, T. Abajyan, B. Abbott, J. Abdallah, S. A. Khalek, R. Aben, B. Abi, M. Abolins, O. AbouZeid, H. Abramowicz, *et al.* (ATLAS Collaboration), Phys. Rev. Lett **111**, 152301 (2013).

[57] T. Lappi, B. Schenke, S. Schlichting, and R. Venugopalan, JHEP **2016**, 61 (2016).

[58] M. Mace, V. V. Skokov, P. Tribedy, and R. Venugopalan, Phys. Rev. Lett. **121**, 052301 (2018).

[59] C. Zhang, C. Marquet, G.-Y. Qin, S.-Y. Wei, and B.-W. Xiao, Phys. Rev. Lett. **122**, 172302 (2019).

[60] J. L. Albacete, H. Petersen, and A. Soto-Ontoso, Phys. Rev. C **95**, 064909 (2017), arXiv:1612.06274 [hep-ph].

[61] F. Gelis, G. Giacalone, P. Guerrero-Rodríguez, C. Marquet, and J.-Y. Ollitrault, arXiv preprint arXiv:1907.10948 (2019).

[62] B. Blok, C. D. Jäkel, M. Strikman, and U. A. Wiedemann, JHEP **12**, 074 (2017), arXiv:1708.08241 [hep-ph].

[63] B. Blok and U. A. Wiedemann, Phys. Lett. B **795**, 259 (2019), arXiv:1812.04113 [hep-ph].

[64] In principle, given the absence of energy loss in colorless particles, the value of v_2 for high-p_T photons [73] or Z^0 bosons should also be sensitive to such initial-state induced anisotropy.

[65] E. Wang and X.-N. Wang, Phys. Rev. Lett. **89**, 162301 (2002), arXiv:hep-ph/0202105.

[66] T. Renk, Phys. Rev. C **74**, 034906 (2006), arXiv:hep-ph/0607166.

[67] Y. He, L.-G. Pang, and X.-N. Wang, Phys. Rev. Lett. **125**, 122301 (2020), arXiv:2001.08273 [hep-ph].

[68] J. G. Milhano and K. C. Zapp, Eur. Phys. J. C **76**, 288 (2016), arXiv:1512.08107 [hep-ph].

[69] A reasonable estimate of the amount of medium induced modification can also be obtained from the ratio between the jet p_T and that of a recoiling colorless trigger boson, although the correlation is not tight even in vacuum due to sizeable out-of-cone radiation [29].

[70] L. Yan, S. Jeon, and C. Gale, Phys. Rev. C **97**, 034914 (2018), arXiv:1707.09519 [nucl-th].

[71] Y. Tachibana, C. Shen, and A. Majumder, (2020), arXiv:2001.08321 [nucl-th].

[72] J. Casalderrey-Solana, J. G. Milhano, D. Pablos, K. Rajagopal, and X. Yao, JHEP **05**, 230 (2021), arXiv:2010.01140 [hep-ph].

[73] A. M. Hamed (STAR), Nucl. Phys. A **931**, 706 (2014), arXiv:1408.0791 [nucl-ex].

Supplemental Material

We show results for jet v_2 in Fig. 4 for PbPb collisions at $\sqrt{s_{NN}} = 2.76$ TeV, using anti-k_t and $R = 0.2$, as a function of centrality (upper panel) and jet p_T for centrality 30-40% (lower panel). The red dots correspond to the results using FES with $60 < p_T < 80$ GeV in the upper panel and $50 < p_T < 210$ GeV in the lower panel, which can be directly compared to ATLAS data [56], in black. Both the centrality and p_T dependence of v_2 measured in experiments can be well described by the hybrid strong/weak coupling model. In addition, we also present the results with IES (with the cuts $p_T > 50$ GeV and $p_T/\chi > 125$ GeV) by green points. As observed in the main text, jet v_2 as a function of the centrality is consistent with zero (upper panel). The p_T-dependence of v_2 is quite similar to the FES when selecting jets above the employed p_T/χ cut, while the more quenched jets below this cut contribute with negative v_2 (lower panel).

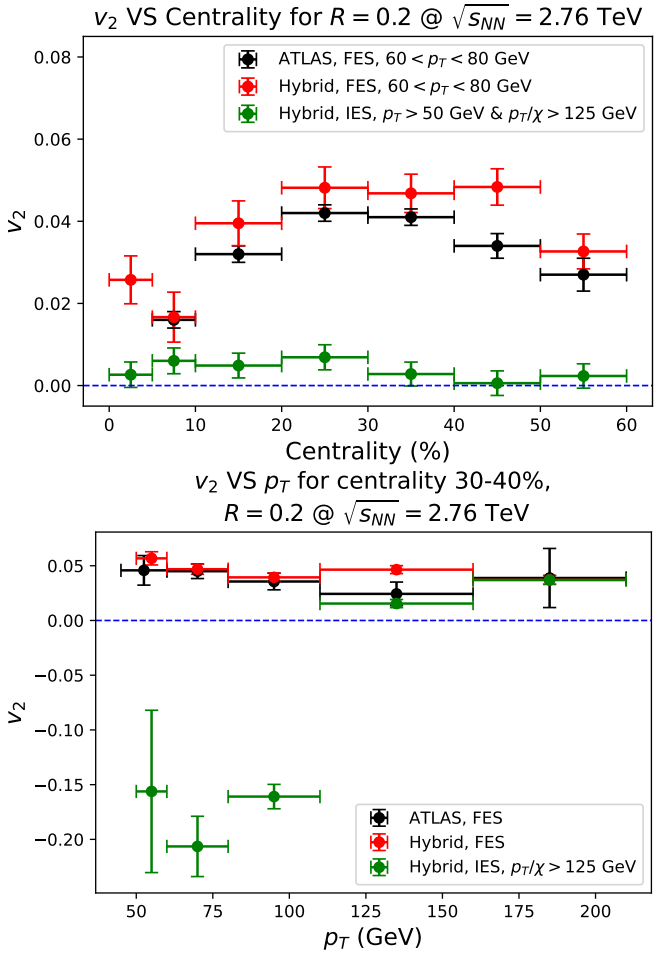

FIG. 4. Top: Centrality dependence of v_2 for FES setup (red) and IES setup with true χ (green). Bottom: p_T dependence of v_2 for FES setup (red) and IES setup with true χ (green). Both results for the FES setup can be directly compared to ATLAS data (black) [56].